Journal of Oceanography, Vol. 63, pp. 293 to 307, 2007

Temporal Variability of Winter Mixed Layer in the Mid- to High-Latitude North Pacific

Eitarou Oka[1]*, Lynne D. Talley[2] and Toshio Suga[1,3]

[1]*Institute of Observational Research for Global Change, Japan Agency for Marine-Earth Science and Technology, Yokosuka, Kanagawa 237-0061, Japan*
[2]*Scripps Institution of Oceanography, University of California, San Diego, La Jolla, CA 92093-0230, U.S.A.*
[3]*Department of Geophysics, Graduate School of Science, Tohoku University, Aoba-ku, Sendai 980-8578, Japan*

(Received 3 February 2006; in revised form 16 November 2006; accepted 20 November 2006)

Temperature and salinity data from 2001 through 2005 from Argo profiling floats have been analyzed to examine the time evolution of the mixed layer depth (MLD) and density in the late fall to early spring in mid to high latitudes of the North Pacific. To examine MLD variations on various time scales from several days to seasonal, relatively small criteria (0.03 kg m^{-3} in density and 0.2°C in temperature) are used to determine MLD. Our analysis emphasizes that maximum MLD in some regions occurs much earlier than expected. We also observe systematic differences in timing between maximum mixed layer depth and density. Specifically, in the formation regions of the Subtropical and Central Mode Waters and in the Bering Sea, where the winter mixed layer is deep, MLD reaches its maximum in late winter (February and March), as expected. In the eastern subarctic North Pacific, however, the shallow, strong, permanent halocline prevents the mixed layer from deepening after early January, resulting in a range of timings of maximum MLD between January and April. In the southern subtropics from 20° to 30°N, where the winter mixed layer is relatively shallow, MLD reaches a maximum even earlier in December-January. In each region, MLD fluctuates on short time scales as it increases from late fall through early winter. Corresponding to this short-term variation, maximum MLD almost always occurs 0 to 100 days earlier than maximum mixed layer density in all regions.

Keywords:
· Winter mixed layer,
· North Pacific,
· temporal variability,
· Argo.

1. Introduction

In mid to high latitudes of the North Pacific, as in the other oceans, the mixed layer reaches its maximum depth in winter, due to surface cooling and wind stirring (Bathen, 1972; Kara *et al*., 2000). In the succeeding seasons, the winter mixed layer is capped by warm and/or fresh surface water, and is left in the subsurface as a vertically homogeneous layer, called a fossil layer (Sprintall and Roemmich, 1999). In the subtropical region, the fossil layer is subducted, and part or all of it irreversibly enters the permanent pycnocline (Stommel, 1979). In particular, thick fossil layers with a large horizontal extent are subducted as mode waters, such as the Subtropical Mode Water (STMW; Masuzawa, 1969), the Central Mode Water (CMW; Nakamura, 1996; Suga *et al*., 1997), and the Eastern Subtropical Mode Water (ESTMW; Hautala and Roemmich, 1998). In the subarctic region including the Bering Sea, where a strong permanent halocline prevents deep convection (Kara *et al*., 2000) and Ekman upwelling predominates (Qiu and Huang, 1995), no pronounced mode waters are found (Hanawa and Talley, 2001). Nevertheless, the lower part of the winter mixed layer remains in the following seasons as a subsurface temperature minimum, which lies at the top of a temperature inversion associated with the strong permanent halocline (Cokelet and Stabeno, 1997; Miura *et al*., 2003; Ueno *et al*., 2005). Thus, the winter mixed layer in mid to high latitudes is essential to the production of various water masses and structures. It is therefore important to properly understand the temporal and spatial

* Corresponding author. E-mail: eoka@ori.u-tokyo.ac.jp
Present address: Ocean Research Institute, The University of Tokyo, Nakano-ku, Tokyo 164-8639, Japan.

variation of its depth and properties.

The spatial variation of the winter mixed layer depth and properties in the North Pacific has been examined in relation to water mass formation in many studies (e.g., Huang and Qiu, 1994; Ladd and Thompson, 2000; Suga *et al*., 2000, 2004; Oka and Suga, 2003). On the other hand, their temporal variation has not been examined in detail, due to a lack of continuous, frequent observations at fixed points. Instead, it has been commonly believed, and often assumed a priori, that both mixed layer depth and density in mid to high latitudes of Northern Hemisphere oceans reach their maximum in late winter, specifically in February and March (e.g., Stommel, 1979; Marshall *et al*., 1993).

Since the factors affecting the mixed layer depth and properties, such as surface heat and freshwater fluxes, horizontal advection, and the ocean structure below the mixed layer (e.g., Tully, 1964; Hanawa and Toba, 1981), vary regionally, the timing of maximum mixed layer depth can also vary regionally. In fact, Takeuchi and Yasuda (2003), using both the climatological temperature and salinity data from the World Ocean Atlas 1998 (Conkright *et al*., 1998) and the temperature time series data of White (1995), demonstrated that in the world oceans at latitudes 20°–30°, the mixed layer depth reaches its maximum around January in the Northern Hemisphere (July in the Southern Hemisphere), which is much earlier than the commonly supposed time frame of February–March (August–September). Furthermore, de Boyer Montégut *et al*. (2004) constructed a global mixed layer depth climatology based on individual temperature and salinity profiles, rather than using averaged profiles as in previous climatologies (e.g., Monterey and Levitus, 1997; Kara *et al*., 2003). In their new climatology, the mixed layer depth in mid to high latitudes of the North Atlantic reaches its maximum in January–February, about one month earlier than the commonly supposed time frame, not only at 20°–30°N, as indicated by Takeuchi and Yasuda (2003), but also at higher latitudes. de Boyer Montégut *et al*. (2004) mentioned that the early occurrence of maximum mixed layer depth is likely due to the temperature/density criterion that they used to determine the mixed layer depth, which is smaller than those used in previous climatological studies and which permits better detection of spring restratification.

Recently, Iwasaka *et al*. (2006) examined temporal variations of the mixed layer depth and properties in the western North Pacific around 24°N, 143°–150°E from December 2001 through August 2002, using temperature and salinity data obtained by a profiling float at a three-day interval. They demonstrated that the mixed layer depth increases from 70 dbar in early December to a maximum of 130 dbar at the end of January, then fluctuates greatly between 30 and 120 dbar until mid-April, decreasing to 20–30 dbar thereafter. In addition to this seasonal change, the mixed layer depth also fluctuates on short time scales with a period of about 10 days, not only between the end of January and mid-April but also in the other periods. Iwasaka *et al*. (2006) mentioned that this high frequency fluctuation might be related to a short-term variation in the surface heat flux, which has a period of 7–10 days.

Since 2000, the international Argo project has deployed profiling floats over the global ocean, with a target density of one per three-degree square, to monitor temperature and salinity down to a depth of 2000 dbar at a 10-day interval (Argo Science Team, 2001). As of July 2005, 494 floats are in operation in the North Pacific, achieving about two-thirds of the target float density. Using the in-situ observation data from these floats during 2001–2005, this paper examines the time evolution of the mixed layer in the late fall to early spring in mid to high latitudes of the North Pacific, with a typical time resolution of several to ten days. Particular attention is paid to the timings of maximum mixed layer depth and density, which are closely related to the formation of water masses and structures.

Since Argo floats do not repeat observations at fixed points (although they drift relatively slowly in most regions), we divide the North Pacific into the smallest possible grid boxes, based on the float density during the analysis period, and treat the float observations in each grid box as quasi-Eulerian measurements. This approach was already used by Ohno *et al*. (2004) for two circular areas with a radius of 150 km, centered at 34°N, 147°E and 44.5°N, 170°E. In this study we expand the analysis area to the whole North Pacific, supported by the recent rapid growth of the Argo float network in the North Pacific.

The data and the definition of the mixed layer depth are explained in Section 2. The structure and timing of the deepest mixed layer in the North Pacific are examined in Section 3. In order to explain the regionally varying distribution of the timing presented in Section 3, the temporal variations of the mixed layer depth and density and the net surface heat flux in each region of the North Pacific are investigated in Section 4. In Section 5 we study how the timing of the deepest mixed layer depends on the definition of the mixed layer depth. A summary and discussion are given in Section 6.

2. Data

We used temperature and salinity data obtained by Argo profiling floats in the North Pacific including the Bering Sea at 0–65°N, 120°E–80°W from August 2001 through July 2005. These floats drift freely at a predetermined parking pressure (typically 1000 dbar), and ascend to the sea surface at a predetermined interval (10 days)

after descending to the maximum pressure (2000 dbar). During the ascent, the floats measure temperature and conductivity at about 60–110 sampling pressures, with a typical sampling interval of 5–10 dbar at depths shallower than 200 dbar, 10–25 dbar at 200–1000 dbar, and 50–100 dbar deeper than 1000 dbar, using a conductivity-temperature-pressure (CTD) sensor module. The collected data are transmitted from the surfaced floats to satellites, and are made freely available within 24 hours, after passing through the Argo real-time quality control (Argo Data Management Team, 2004).

The accuracy of SBE-41 and SBE-41CP CTD sensor modules, which are supplied by Sea-Bird Electronics, Inc. and mounted on more than 95% of the floats in the North Pacific, is 0.002°C in temperature, 0.005 in equivalent salinity, and 2.4 dbar in pressure, according to the manufacturer. The accuracy in equivalent salinity for floats a few years after their deployment might be as large as 0.01, which is the target accuracy of Argo (Argo Science Team, 2000), because recovery of four operating floats and recalibration of their sensors indicated that a negative salinity drift increases with time, at a rate of -0.004 yr^{-1} (Oka and Ando, 2004; Oka, 2005).

The real-time quality controlled data were downloaded from the ftp site of Argo Global Data Center. About 40% of the data in 2001 have also passed through the Argo delay-mode quality control (Argo Data Management Team, 2002; Wong *et al.*, 2003; Wong and King, 2005). From these data we first eliminated profiles with fewer than 20 sampling layers, the vertical resolution of which is expected to be lower than the typical standard hydrographic observations, and deleted layers in each profile at which temperature, salinity, or pressure was flagged as bad or probably bad. We then visually inspected each profile, and removed defective ones, such as those with a shallowest level much deeper than 10 dbar, those lacking intermediate layers for certain depths, and those with obviously bad temperature, salinity, or pressure values. These procedures finally selected 35,804 profiles for the four year period. The selected data were used after each profile was interpolated on a 1-dbar grid using the Akima spline (Akima, 1970), and potential temperature and density (called temperature and density henceforth) referred to 0 dbar were calculated from the interpolated temperature and salinity data.

The definition of the mixed layer depth (MLD) is critical to the results of this study, as demonstrated later in Section 5. We defined MLD as the shallower value of the depth at which density increases by 0.03 kg m^{-3} from the sea surface and that at which temperature decreases or increases by 0.2°C from the surface. Both the density and temperature criteria were employed by de Boyer Montégut *et al.* (2004) to estimate the depth through which surface fluxes have been mixed within the last few days.

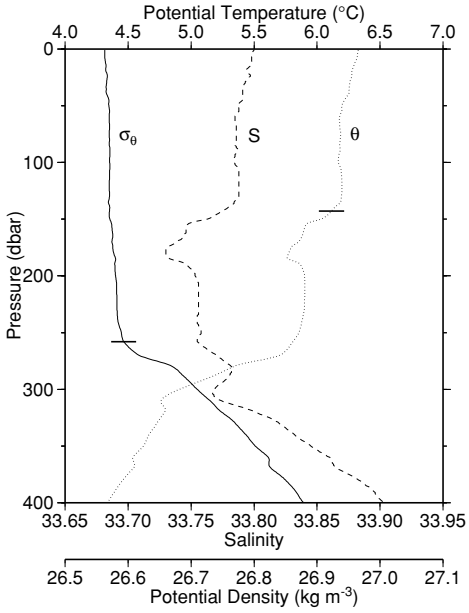

Fig. 1. Vertical profile of potential temperature (dotted curve), salinity (dashed curve), and potential density (solid curve), obtained at 43.13°N, 158.97°E on 6 April 2005 by an Argo float. Thick solid lines denote the MLD calculated by the density criterion of 0.03 kg m^{-3} (258 dbar) and that from the temperature criterion of 0.2°C (143 dbar).

We adopted these criteria to clarify MLD variations on various time scales from several days to seasonal, such as the one shown by Iwasaka *et al.* (2006).

As mentioned in de Boyer Montégut *et al.* (2004), temperature criteria can overestimate MLDs in regions of barrier layers (e.g., Lukas and Lindstrom, 1991), while density criteria can overestimate them in regions of "compensated layers" just beneath the mixed layer, where density is very close to the mixed layer value while both temperature and salinity are different (Fig. 1). To avoid either overestimate, we used both criteria together, thanks to the advantage of Argo float data, which report both temperature and salinity. As a result, MLDs of 88% of profiles were determined by the density criterion, and 12% by the temperature criterion.

Values of temperature, salinity, and density at 10 dbar were used as the surface values. This is because the floats do not conduct measurements at depths shallower than several decibars, to avoid fouling of the conductivity sensor at the sea surface, and also because, if shallower values are used, the depth of a diurnal pycnocline near the surface might be detected rather than MLD (de Boyer Montégut *et al.*, 2004). The temperature, salinity, and density values at the surface were considered to represent those of the mixed layer, which is justified by the

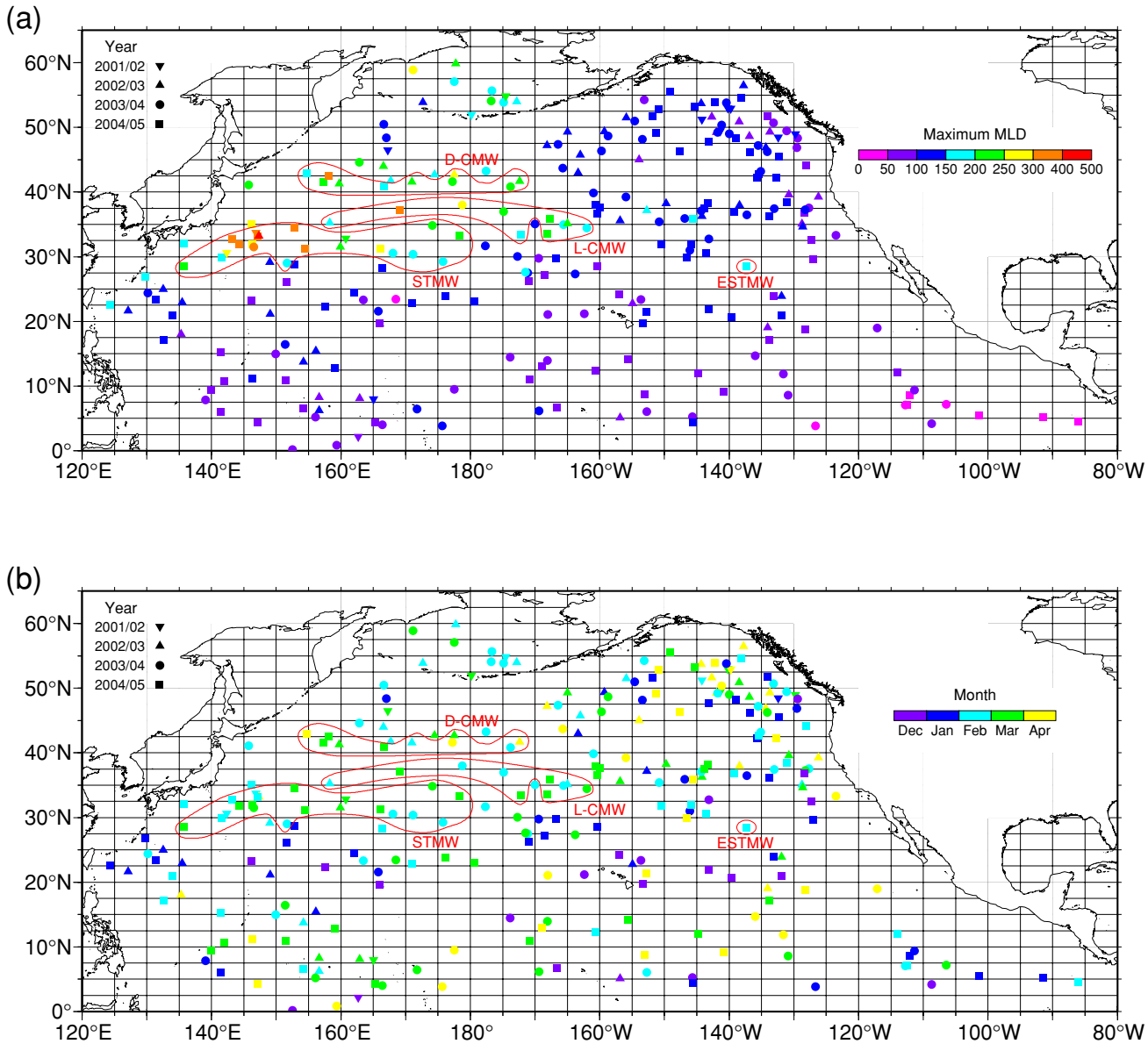

Fig. 2. Maximum MLD (a) and the month of its occurrence (b) in each grid box during December–April of 2001/02 (inverted triangles), 2002/03 (triangles), 2003/04 (circles), and 2004/05 (squares). These are plotted at the location where they were observed. Red curves enclose the mode water formation regions.

smallness of both the temperature and density criteria.

The daily mean reanalysis data of net surface heat flux, which is the sum of short and long wave radiation fluxes and sensible and latent heat fluxes, were downloaded from the website of the National Centers for Environment Prediction and the National Center for Atmospheric Research (NCEP/NCAR; Kistler *et al.*, 2001). These data, provided on a 1.90° × 1.875° (latitude, longitude) grid, were linearly interpolated on a 0.1° × 0.1° grid and then averaged over each 2.5° × 5° grid box.

3. Structure and Timing of Deepest Winter Mixed Layer

The North Pacific is divided into 2.5° × 5° (latitude, longitude) grid boxes, in each of which the float observations are regarded as quasi-Eulerian measurements. Considering a single grid box, if the observations were conducted in both halves of all five months from December through April in a particular year, we consider that the grid box was continuously observed during that late fall to early spring period. For each of such continuously ob-

Table 1. Number of grid boxes, and potential temperature (ϑ), salinity (S), and potential density (σ_θ) at the sea surface for the deep mixed layers in the mode water formation regions.

Water type	No.	ϑ (°C)	S	σ_θ (kg m^{-3})
STMW	21	15.4–19.7	34.63–34.98	24.76–25.61
L-CMW	10	12.0–14.4	34.32–34.58	25.72–26.12
D-CMW	10	6.0–10.2	33.73–34.20	26.24–26.57
ESTMW	1	19.0	34.94	24.98

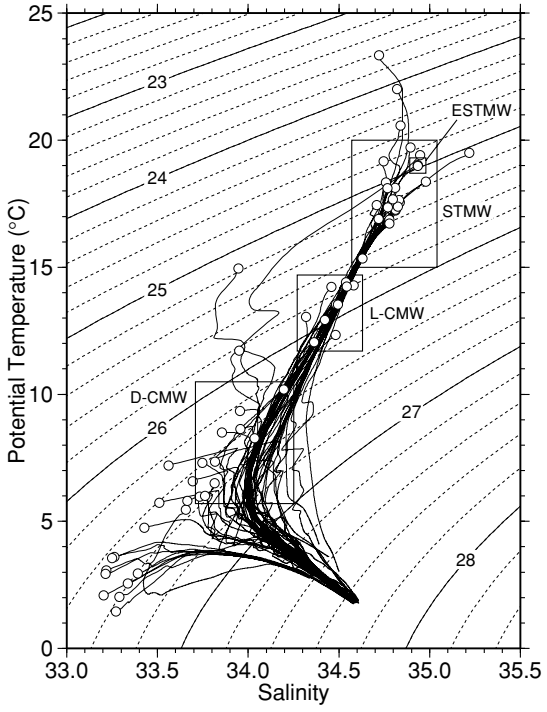

Fig. 3. Potential temperature-salinity relations at the sea surface (circles) and below it (solid curve) for the observation points in Fig. 2(a) where the maximum MLD exceeds 150 dbar. Solid squares indicate the property ranges of mode waters. Solid and dashed contours denote potential density (kg m^{-3}).

served grid boxes, 14 in number (winter of 2001/02), 53 (2002/03), 90 (2003/04), and 107 (2004/05), we searched for the maximum MLD and the month of its occurrence (Fig. 2). Even if the analyzed period of December–April is extended by one month to May or back to November, the month distribution in Fig. 2(b) remains virtually unchanged north of 20°N, which is the region of our interest.

The maximum MLD exceeds 150 dbar east of Japan at 27.5°–45°N, west of 160°W as well as in the Bering Sea (Fig. 2(a)). The deep mixed layers east of Japan are classified, according to their temperature, salinity, and density (Fig. 3 and Table 1), into the formation region of STMW* south of the Kuroshio Extension (Suga and Hanawa, 1990; Bingham, 1992; Oka and Suga, 2003) and that of CMW north of the Kuroshio Extension (Nakamura, 1996; Suga *et al*., 1997, 2004). The latter region is further divided into the formation regions of the lighter and denser varieties of CMW (L-CMW and D-CMW; Oka and Suga, 2005) south and north of the Kuroshio bifurcation, respectively. The five mixed layers deeper than 150 dbar at 42°–45°N, 163°E–178°W north of the D-CMW formation region have densities (26.26–26.52 kg m^{-3}) similar to D-CMW but lower salinities (33.43–33.70), and are accompanied by a sharp halocline and a temperature inversion beneath, which appear on the temperature-salinity diagram as a large increase of salinity with a slight increase of temperature (Fig. 3). The corresponding grid boxes are judged to be located in the subarctic region north of the subarctic frontal zone (Yuan and Talley, 1996), and are not included in the D-CMW formation region. The wavy northern boundary of the D-CMW formation region is considered to reflect high spatial and temporal variability of the subarctic frontal zone. The deep mixed layer corresponding to the formation region of ESTMW is found in only one grid box at 27.5°–30°N, 140°–135°W in 2004/05. This is probably because the observation density around this grid box, namely in the ESTMW formation region, is relatively low.

Outside the deep mixed layer regions, the maximum MLD in mid to high latitudes is between 100 and 150 dbar, except along the west coast of North America where it is slightly less than 100 dbar (Fig. 2). The maximum MLD tends to decrease equatorward south of 30°N, and

*The deep mixed layer reaching 283 dbar at 35°N, 146°E in 2004/05 has properties of STMW, but the time series of mixed layer properties in the corresponding grid box at 35°–37.5°N, 145°–150°E indicates that this grid box contains similar proportions of two different types of water north and south of the Kuroshio Extension. Accordingly, the grid box is excluded from the STMW formation region.

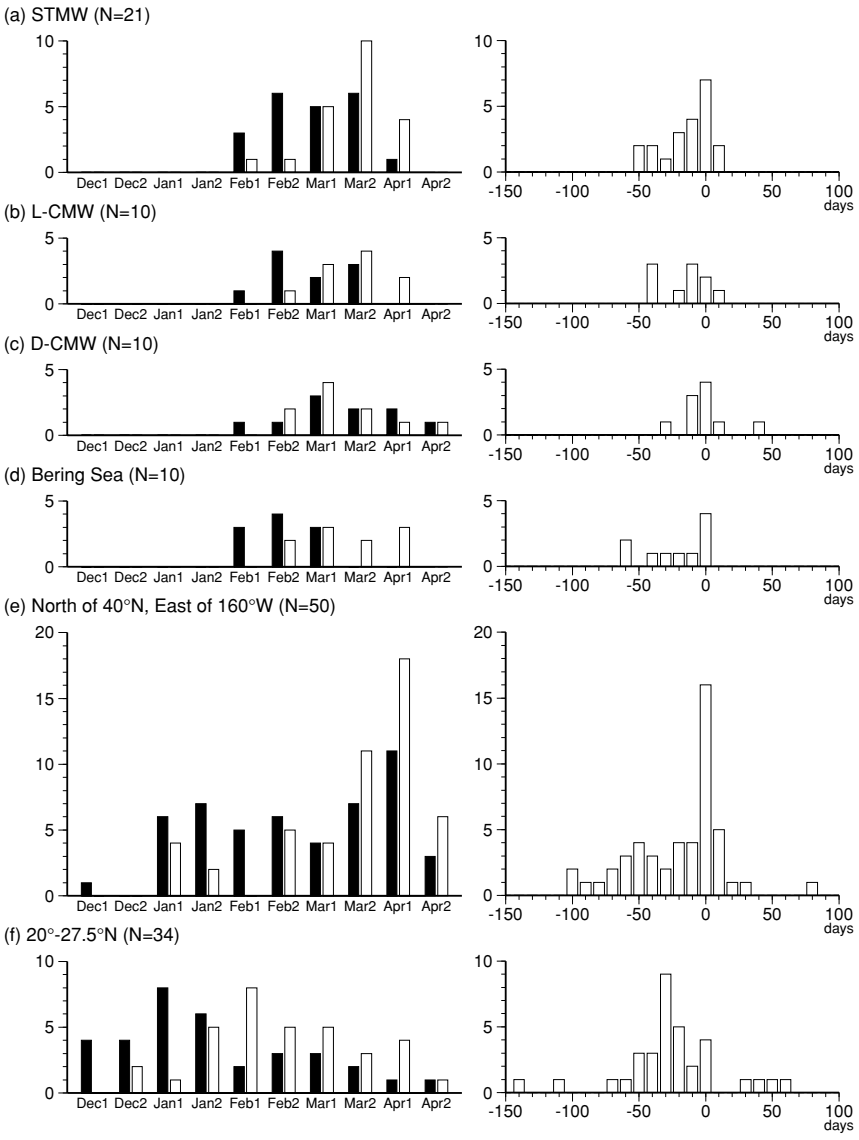

Fig. 4. Histogram of timing of the maximum MLD (black bars; left) and maximum mixed layer density (white bars; left) and difference between the two timings (right) for grid boxes in each region: formation regions of (a) STMW, (b) L-CMW, and (c) D-CMW; (d) Bering Sea; (e) north of 40°N, east of 160°W; and (f) between 20° and 27.5°N. "Dec1" and "Dec2" on the abscissa in the left panels indicate the first and second halves of December, respectively, and so on for the other months. In the right panels, positive differences indicate that the maximum mixed layer density precedes the maximum MLD.

is mostly less than 100 dbar south of 20°N, with particularly low values (less than 50 dbar) in the eastern equatorial Pacific south of 10°N, east of 130°W.

The month of maximum MLD varies greatly, between December and April, over the North Pacific (Fig. 2(b)). Nevertheless, it shows a coherent distribution in particular regions. In the STMW and L-CMW formation regions, MLD reaches its maximum mostly in February and March, which agrees with the previously supposed time frame (Fig. 4, black bar in left panels). The average dates of maximum MLD, calculated for 21 grid boxes in the STMW formation region and 10 grid boxes in the L-CMW formation region, are 5 and 4 March, respectively (Table 2). In the D-CMW formation region (10 grid boxes) to the north, MLD is at its maximum in February through April, with an average date of 16 March. This is consistent with an intuitive idea that the higher the latitude, the later spring restratification starts. However, in the Bering Sea (10 grid boxes), where the maximum MLD is also fairly large, MLD reaches the maximum in February and the first half of March, with an average date of 23 February. This is 10–20 days earlier than the STMW and CMW

Table 2. Number of grid boxes, and averages (standard deviations in days) of dates of maximum MLD and maximum mixed layer density and the difference between the two dates for each region in Fig. 4. Positive differences in the rightmost column indicate that the maximum mixed layer density precedes the maximum MLD.

Region	No.	Maximum MLD	Maximum density	Difference
STMW	21	5 Mar. (16)	19 Mar. (14)	–14
L-CMW	10	4 Mar. (14)	21 Mar. (11)	–17
D-CMW	10	16 Mar. (22)	17 Mar. (19)	–1
Bering Sea	10	23 Feb. (10)	18 Mar. (18)	–23
North of 40°N, East of 160°W	50	28 Feb. (34)	21 Mar. (29)	–21
20°–27.5°N	34	27 Jan. (36)	21 Feb. (29)	–26

formation regions, in spite of the even higher latitudes.

In contrast to the above regions, the eastern subarctic North Pacific north of 40°N, east of 160°W (50 grid boxes), where the float density has been relatively high since the early stage of Argo (Freeland and Cummins, 2005), is characterized by various timings of maximum MLD between January and April, the most frequent occurrence being in the first half of April. The average date of maximum MLD is 28 February, which is somewhat earlier than the STMW and CMW formation regions to the southwest.

Just south of the STMW formation region and the single grid box for the ESTMW formation region, there is a zonal band between 20° and 30°N in the southern subtropics where MLD reaches its maximum primarily in December and January. This is consistent with Takeuchi and Yasuda's (2003) finding that the mixed layer in this latitude band shoals during winter, from January to March. The average date of maximum MLD, calculated for a latitude band of 20°–27.5°N* (34 grid boxes), is 27 January, which is 1–1.5 months earlier than the five northern regions. These time lags are all significant at the 99% confidence level, according to Student's *t*-test.

South of 20°N, MLD exhibits less seasonality than the northern regions. We made a preliminary calculation of the timing of maximum MLD in the same way as Fig. 2(b), but for a one-year period from August through July and for larger grid boxes of 5° × 10° (not shown). The maximum MLD occurs mostly between January through April north of 20°N, as in Fig. 2(b), but it occurs for a longer period from January through July at 10°–20°N and in every month except June at 0°–10°N. Since our interest is in the winter mixed layer evolution in mid to high latitudes, we do not pursue the mixed layer variations south of 20°N in the remainder of the paper.

*The latitude of 27.5°N was chosen as the northern limit of this latitude band, rather than 30°N, to avoid overlap with the STMW and ESTMW formation regions.

The mixed layer density reaches its maximum mostly between the second half of February and the first half of April in the STMW and CMW formation regions and the Bering Sea, and in a slightly wider time frame in the eastern subarctic North Pacific (Fig. 4, white bar in left panels). The average dates of maximum mixed layer density in these five regions north of 30°N are concentrated between 17 and 21 March (Table 2). In the southern subtropics between 20° and 27.5°N, the mixed layer density is at its maximum in a yet wider range between the second half of December and April. The average date is 21 February, which is one month earlier than the five northern regions (all significant at the 99% level). The southern subtropics are characterized not only by the early maximum MLD but also by the early maximum mixed layer density.

In each region there is a tendency for MLD to reach its maximum earlier than the mixed layer density (Fig. 4, left panels). In other words, MLD tends to reach its maximum while the mixed layer density is still increasing. This tendency is true for individual grid boxes; the difference between the dates of the two maxima is mostly null or negative, which means that the MLD maximum occurs earlier (Fig. 4, right panels). The average date of maximum MLD corresponds to that of maximum mixed layer density in the D-CMW formation region, but the former precedes the latter by 14–26 days in the other regions, all of which are significant at the 99% level (Table 2).

Takeuchi and Yasuda (2003) demonstrated that the mixed layer shoaling at 20°–30°N from January to February is mostly accompanied by a decrease of the mixed layer temperature, i.e., an increase of the mixed layer density. The float observations suggest that this relation applies to the higher latitudes, too. In the next section we examine the temporal variations of the mixed layer depth and density and the surface heat flux in each region, to understand what causes the difference in the timing of maximum MLD among regions and that in the timing between the maximum MLD and the maximum mixed layer density in each region.

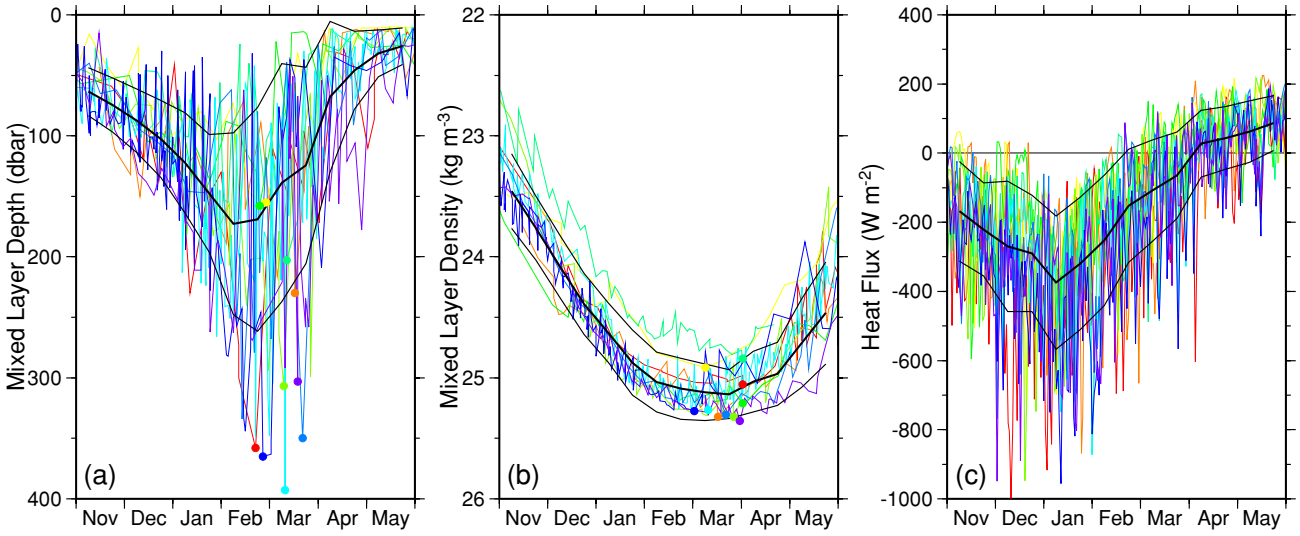

Fig. 5. Time series of (a) MLD, (b) mixed layer density, and (c) net surface heat flux in 10 grid boxes in the STMW formation region during November through May of 2001/02–2004/05 (colored curves) plotted against observation month. Each grid box is represented by a different color. Colored dots in (a) and (b) denote the maximum MLD and mixed layer density for each grid box. Thick and thin black curves in each panel indicate the mean and standard deviation for each half-month period, calculated for all grid boxes in the region. Note that MLD and the mixed layer density increase downward on the ordinate.

4. Time Evolution of Winter Mixed Layer in Each Region

Figure 5 shows time series of MLD, the mixed layer density, and the net surface heat flux in each grid box in the STMW formation region from November through May, along with their averages and standard deviations for all 21 grid boxes for each half-month period. To make the figures clear, the time series are presented only for 10 randomly-chosen grid boxes, but the features mentioned below also apply to the other grid boxes.

A striking feature revealed by in-situ Argo float observations is that MLD fluctuates not only seasonally but also on short time scales with periods much shorter than a month, as demonstrated by Iwasaka *et al*. (2006). These short-term variations of MLD partly reflect the spatial variation of MLD within each grid box, particularly when the box is occupied by more than one float. However, they are observed even in grid boxes containing one float, in which the influence of spatial variation of MLD is expected to be minimal. Therefore, such short-term variations of MLD are considered an intrinsic feature of the mixed layer. These variations can be caused by: (1) short-term variations of surface heat flux (Iwasaka *et al*., 2006); (2) non-uniform stratification below the mixed layer through which the mixed layer is deepening; (3) vertical movement of the structure below the mixed layer due to internal waves (Tully, 1964); and (4) horizontal advection or mixing that destroys the vertical homogeneity of the mixed layer and temporarily decreases MLD.

From November through the first half of February, MLD increases with the short-term fluctuations, due to strong surface cooling. In the second half of February through March, MLD becomes even larger and reaches its maximum in each grid box, while at the same time relatively small MLDs are observed with increasing frequency, so the amplitude of short-term variations becomes large. These are reflected in the large standard deviation of MLD and the decrease of average MLD. During this period, the surface heat flux is mostly negative, but occasionally turns positive. These warming events can restratify the mixed layer and decrease MLD temporarily. In April and May the surface heat flux becomes predominantly positive, and MLD decreases steeply to less than several tens of decibars. Thus, the temporal variation of MLD can be divided into three stages, and the variation in each stage is consistent with that of surface heat flux. Iwasaka *et al*. (2006) demonstrated that the MLD variation south of the STMW formation region from December through the following August can be divided into three stages in a similar manner, and is consistent with the variation of surface heat flux.

In contrast to MLD, the mixed layer density changes relatively gradually, with short-term variations much smaller than the seasonal ones. It increases rapidly from November through the first half of February, then slowly until mid to late March, decreasing thereafter. These three periods, with different rates of change, correspond broadly to the three stages defined above in terms of MLD varia-

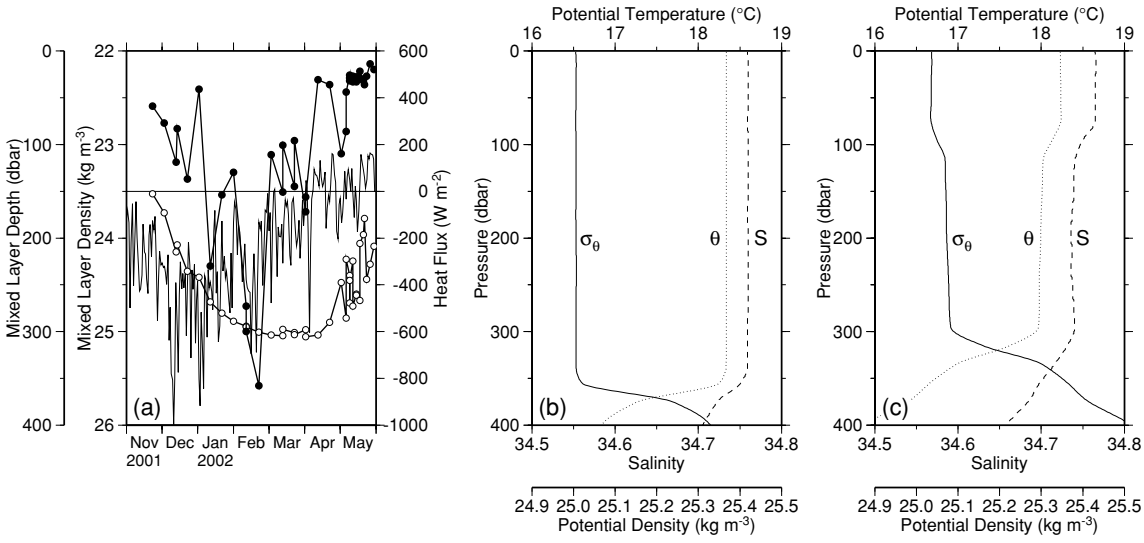

Fig. 6. (a) Time series of MLD (thick curve with black circles), mixed layer density (thin curve with white circles), and net surface heat flux (thin curve) in a grid box at 32.5°–35°N, 145°–150°E in 2001/02. (b) and (c) Vertical profile of potential temperature (dotted curve), salinity (dashed curve), and potential density (solid curve) obtained at (b) 33.75°N, 146.83°E on 21 February 2002 and (c) 33.81°N, 146.69°E on 3 March 2002 in the grid box.

tion. The variation of the mixed layer density is also consistent with that of net surface heat flux, which, on average, is negative and large in the first stage, decreasing in magnitude in the second stage, and becoming positive in the third stage.

Both MLD and the mixed layer density reach their maximum in the second stage around the second half of February through March, but their behavior during the stage is quite different. While the mixed layer density continues to increase gradually, MLD changes significantly on short time scales. As a result, the maximum MLD almost always occurs earlier than the maximum mixed layer density, which appears as negative time lags in Fig. 4(a) (right panel).

In some grid boxes, the precedence of the maximum MLD seems to be caused by horizontal advection. In a grid box at 32.5°–35°N, 145°–150°E in 2001/02, the mixed layer density reaches a maximum of 25.06 kg m^{-3} on 2 April, approximately when the surface heat flux changes from negative to positive (Fig. 6(a)). Preceding this by 40 days, MLD reaches a maximum of 358 dbar on 21 February. It then decreases to 111 dbar ten days later on 3 March, remains between 100 and 170 dbar for about one month, and finally drops to 30 dbar on 12 April. The large decrease of MLD from 21 February to 3 March occurs in such a way that the deep mixed layer is broken into two layers above and below 100 dbar (Figs. 6(b) and (c)). Since the surface heat flux remains negative and the mixed layer density (temperature) increases (decreases) slightly between the two observations, the destruction of the deep mixed layer is not likely to be due to surface heating. Rather, the warmer, saltier water shallower than 100 dbar, or the colder, fresher water deeper than 100 dbar—more likely the former—is expected to be advected from a neighboring region.

MLD in the eastern subarctic North Pacific north of 40°N, east of 160°W stops increasing on average at a relatively early stage of winter around early January, subsequently remaining relatively constant until early April (Fig. 7). This is because the shallow, strong halocline at depths of 100–200 dbar in this region (Uda, 1963) prevents the mixed layer from deepening further (Tully, 1964). During the period of relatively constant MLD, MLD fluctuates on short time scales, reaching its maximum at various times, as shown in Fig. 4(e) (left panel). On the other hand, the mixed layer density gradually increases until the end of the period, in association with small but negative surface heat flux, on average. As a result, again, the maximum MLD typically occurs earlier than the maximum mixed layer density.

Temporal variations of MLD in the southern subtropics between 20° and 27.5°N are different from the northern regions in many respects (Fig. 8). First, MLD reaches its maximum in early winter around December and January in most of the grid boxes, as shown in the previous section. Meanwhile, small MLDs are frequently observed during these two months, and a systematic increase of MLD from late fall to early winter is not seen as in the other regions. Rather, the mixed layer deepens somewhat sporadically. Furthermore, as emphasized by Takeuchi and

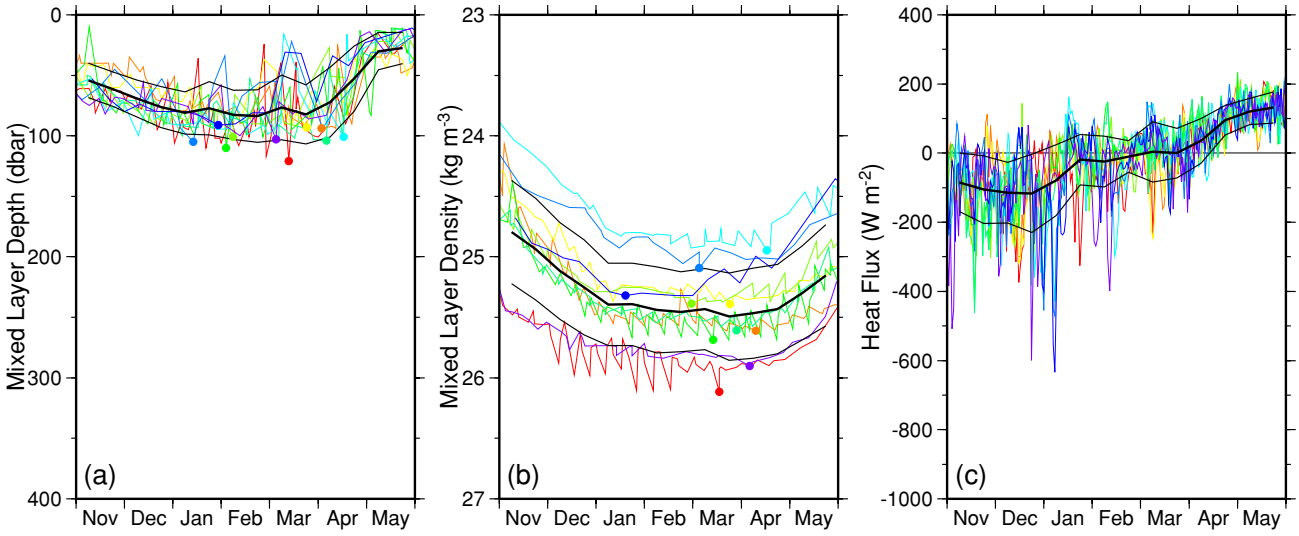

Fig. 7. Time series for the region north of 40°N, east of 160°W, otherwise following Fig. 5.

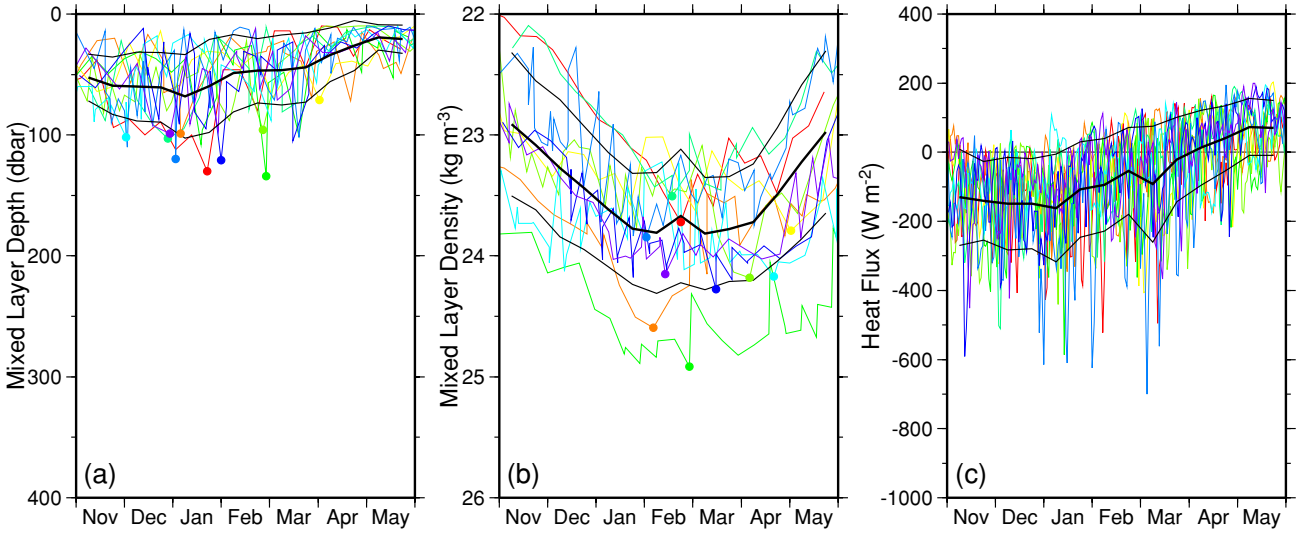

Fig. 8. Time series for the region between 20° and 27.5°N, otherwise following Fig. 5.

Yasuda (2003), MLD reaches its maximum while the mixed layer density increases at a considerable rate. Although our analysis has shown that MLD also reaches its maximum while the mixed layer density increases in the other regions, the difference between the maximum mixed layer density and the mixed layer density at the time of the maximum MLD is small, being 0.08 kg m^{-3} on average in both the SMTW formation region and the eastern subarctic North Pacific. In the southern subtropics the difference is as large as 0.44 kg m^{-3}, which indicates that the MLD decrease after the maximum has been attained is accompanied by a significant increase of the mixed layer density.

What causes the early MLD maximum and the subsequent MLD decrease with increasing mixed layer density in this region? One possibility is temporal surface heating in early winter, but this is not likely to be the primary cause because the frequency of positive surface heat flux during December and January is low. Another possibility is horizontal processes, which is suggested by the mixed layer shoaling with increasing mixed layer density (Takeuchi, 2006). After analyzing the output of the

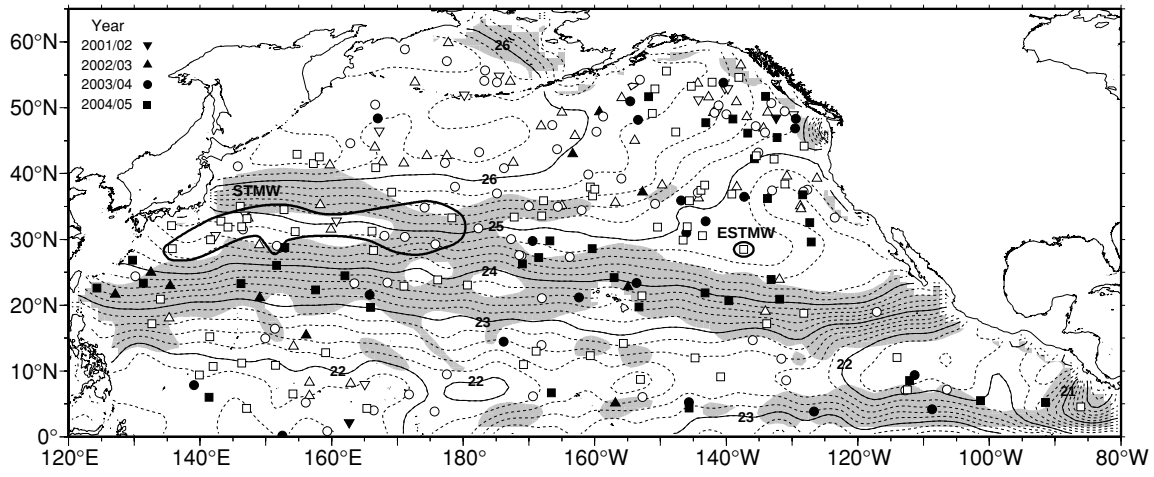

Fig. 9. Sea surface density distribution in the North Pacific in January from the World Ocean Atlas 2001 climatology (Conkright *et al.*, 2002). Region of horizontal density gradient greater than 1.2×10^{-6} kg m^{-4} is shaded. Superimposed are the locations of the maximum MLD in each grid box during December–April of 2001/02 (inverted triangles), 2002/03 (triangles), 2003/04 (circles), and 2004/05 (squares), with black (white) symbols for the grid box where the maximum MLD occurs in December and January (February–April). Thick curves denote the STMW and ESTMW formation regions.

high-resolution OFES model (Masumoto *et al.*, 2004), Takeuchi (2006) pointed out that eddies propagating westward in this latitude band might cause the early MLD maximum by raising the main thermocline just below the mixed layer.

Horizontal advection or mixing can also contribute to the destruction of the winter mixed layer, as shown for the STMW formation region. The winter mixed layer in this region has a strong northward density gradient (reflected in large, short-term variations of the mixed layer density in some grid boxes containing more than one Argo float (Fig. 8(b))), in contrast to the relatively weak horizontal gradient in the STMW and ESTMW formation regions just to the north (Fig. 9). Such a mixed layer structure might be favorable for the destruction of the winter mixed layer by horizontal advection/mixing. If this destructive effect exceeds the mixed layer deepening due to negative surface heat flux, particularly in late winter when the negative heat flux is small, it is likely that the mixed layer will hardly be able to develop fully. This might explain the sporadic mixed layer deepening and the early MLD maximum in this region.

This latitude band is also characterized by the early mixed layer density maximum around February, which is about one month earlier than the northern regions (Figs. 4 and 8(b) and Table 2). However, this does not agree with the temporal variation of surface heat flux, which changes from negative to positive in April on average, as in the northern regions (Fig. 8(c)). Even if we calculate the ocean's net density gain considering Ekman density transport, the ocean between 20° and 30°N gains density until March and starts to lose it in April, as in the latitude band of 30°–40°N to the north (Fig. 10). A possible explanation for this inconsistency is that negative Ekman density transport in the southern part of the 20°–30°N latitude band in winter (not shown), due to northward Ekman flow, is actually much larger than that based on climatology, due to locally or temporally enhanced wind stress and/or meridional surface density gradient, and the ocean in that area actually starts to lose density much earlier than April. Further studies are needed to clarify the mechanism of mixed layer variability in this latitude band, which seems to be related to the formation of the North Pacific Tropical Water (Cannon, 1966) occurring at 20°–30°N, 140°E–140°W (Suga *et al.*, 2000).

5. Comparison with Results using Larger Criterion

As the criterion to determine MLD, Levitus (1982) adopted a temperature value of 0.5°C and a density value of 0.125 kg m^{-3}, which corresponds to a temperature change of 0.5°C in a temperature range of 17°–19°C with salinity of about 35.0. Since then, both criteria have been used in a number of studies. However, they were originally adopted rather arbitrarily for the averaged temperature and salinity profiles from climatologies, and seem to be somewhat too large to be used for individual CTD profiles with fine vertical resolution. If such large criteria are used for individual profiles, they can overestimate MLDs and might fail to properly detect temporal variations of MLD (de Boyer Montégut *et al.*, 2004).

Our analysis using in-situ Argo float data has revealed the regional difference in the timing of maximum

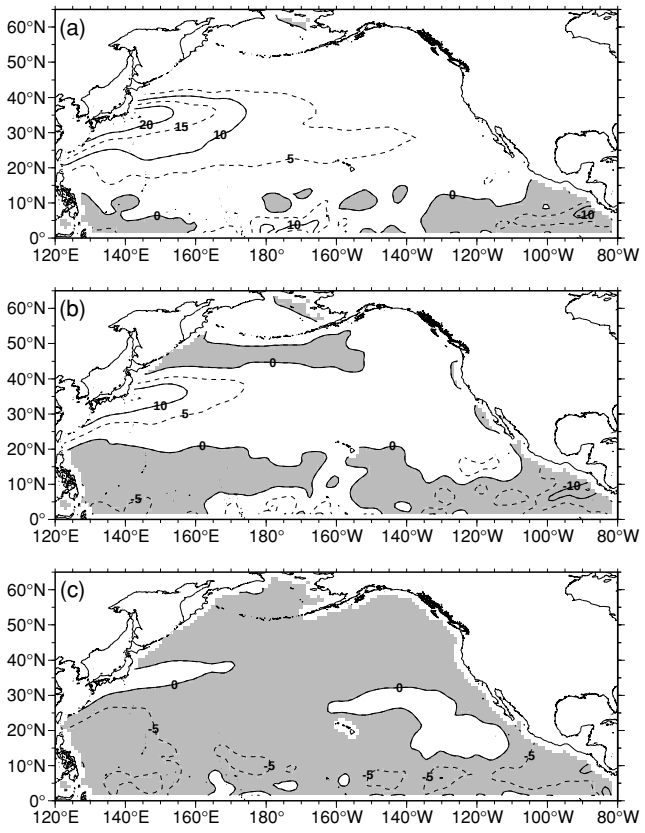

Fig. 10. Net density gain (10^{-6} kg m^{-2}s^{-1}) by the North Pacific ocean due to the surface density flux and the Ekman density transport in (a) February, (b) March, and (c) April, calculated using monthly climatologies of surface heat and freshwater fluxes and wind stress from da Silva *et al.* (1994) and those of surface temperature and salinity from the World Ocean Atlas 2001 (Conkright *et al.*, 2002). Negative values are shaded.

MLD, which is reflected in its latitudinal difference (Fig. 11(a)). The maximum MLD occurs most frequently in February–March at 30°–40°N where the STMW and L-CMW formation regions are located, a little earlier in February at 50°–60°N including the Bering Sea, and much earlier in January at 20°–30°N. At 40°–50°N, the frequency of maximum MLD is highest in February–March, as at 30°–40°N, but it is relatively constant between January and April, reflecting the MLD variations in the eastern subarctic North Pacific.

When we repeat the calculation using the 0.125 kg m^{-3} and 0.5°C criteria, instead of our values of 0.03 kg m^{-3} and 0.2°C, we obtain a quite different result (Fig. 11(b)). The maximum MLD occurs most frequently in March in every latitude band, and the early maximum at 20°–30°N no longer appears. This implies that such large criteria cannot detect spring restratification well, as pointed out by de Boyer Montégut *et al.* (2004). When we compute MLDs from individual CTD profiles including those from Argo floats, we need to use an adequately small criterion to properly understand temporal variations of MLD.

Meanwhile, although we used a similar small criterion to that adopted by de Boyer Montégut *et al.* (2004), our result does not agree with their finding that MLD in the whole mid- to high-latitude North Atlantic reaches its maximum in January–February, about one month earlier than the commonly supposed time frame. In our result for the North Pacific, the maximum MLD occurs significantly earlier than the commonly supposed time frame at 20°–30°N, but not at higher latitudes (Fig. 11(a)). This discrepancy might be because the target ocean is different, and/or because the timing of maximum MLD is computed in a different way; while we used the time series of

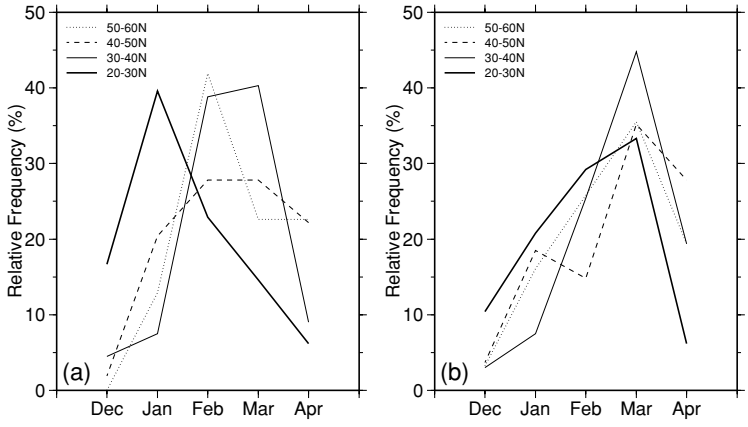

Fig. 11. (a) Relative frequency of the month of maximum MLD in each 10-degree latitude band between 20° and 60°N, based on the month distribution of Fig. 2(b). (b) As (a) but for MLD determined using a density criterion of 0.125 kg m^{-3} and a temperature one of 0.5°C, instead of 0.03 kg m^{-3} and 0.2°C used in Section 2.

MLD directly, de Boyer Montégut *et al*. (2004) used monthly MLD in each 2° × 2° grid box, defined as the median of MLDs in the grid box.

6. Summary and Discussion

Temperature and salinity data during 2001–2005 from Argo profiling floats were analyzed to examine the time evolution of the mixed layer in the late fall to early spring in mid to high latitudes of the North Pacific. In the STMW and CMW formation regions and in the Bering Sea, MLD reaches its maximum mostly in February and March, which agrees with the previously supposed time frame. In the eastern subarctic North Pacific, where the strong permanent halocline prevents the mixed layer from deepening further at a relatively early stage of winter, MLD varies little from early January through early April, leading to various timings of maximum MLD during this period. Between 20° and 30°N, MLD reaches its maximum primarily in December and January. This is consistent with Takeuchi and Yasuda's (2003) finding that the mixed layer in this latitude band shoals during winter.

In each region, MLD fluctuates on short time scales as it increases from late fall through early winter, in contrast to the mixed layer density, which increases relatively gradually. Corresponding to this short-term variation and also possibly due to destruction of the mixed layer by horizontal advection, MLD tends to reach its maximum earlier than the mixed layer density, by up to several tens of days. In other words, MLD reaches its maximum while the mixed layer density is still increasing. The increase of the mixed layer density after the maximum MLD has been attained is particularly large at 20°–30°N, which also agrees with Takeuchi and Yasuda's (2003) result.

These results were obtained using adequately small criteria of 0.03 kg m^{-3} and 0.2°C to determine MLD. If larger, historical criteria of 0.125 kg m^{-3} and 0.5°C are used instead, we do not obtain such regionally varying timings of maximum MLD; in that case, MLD reaches its maximum most frequently in March in every latitude band, which corresponds with the previously supposed time frame.

The present analysis reveals that the temporal variation of winter MLD differs from region to region, with the maximum MLD occurring in various months, and that MLD is often noisy. Such spatial/temporal variability of MLD, together with its mesoscale spatial variability (e.g., Uehara *et al*., 2003), should be considered in future mixed layer studies in the Argo era, in which enormous numbers of CTD profiles are continuously obtained with high spatial/temporal resolution. In addition to the seasonal and shorter-term variations, MLD is known to exhibit interannual variations (e.g., Ohno *et al*., 2004; Wirts and Johnson, 2005), decadal variations (e.g., Yasuda *et al*., 2000), and even longer trends (e.g., Freeland *et al*., 1997). In a year or two we shall be able to examine such long-term variations in detail on a basin scale, thanks to the completion of the Argo float array.

Acknowledgements

The authors are grateful to Tsuyoshi Ohira for his help in preparing the Argo float data. They also thank Kanako Sato, Hiromichi Ueno, Masaki Kawabe, and an anonymous reviewer for helpful comments on the manuscript. This work was done while EO was staying at Scripps Institution of Oceanography (SIO) as a visiting scholar. He thanks Nobuo Suginohara and Nobuyuki Shikama for giving him an opportunity to visit SIO and Tomomi Ushii, the administrative assistant at SIO, for her extraordinary support for him and his family during their stay at SIO. TS was partly supported by the Japan Society of Promotion of Science (Grant-in-Aid for Scientific Research (B), No. 16340135). The Argo float data used in this study were collected and made freely available by the International Argo Project and the national programs that contribute to it (http://www.argo.ucsd.edu, http://argo.jcommops.org). Argo is a pilot program of the Global Ocean Observing System.

References

Akima, H. (1970): A new method of interpolation and smooth curve fitting based on local procedures. *J. Assoc. Comput. Meth.*, **17**, 589–603.

Argo Data Management Team (2002): Report of the Argo Data Management Meeting. *Proc. Argo Data Management Third Meeting*, Marine Environmental Data, Ottawa, ON, Canada, 42 pp.

Argo Data Management Team (2004): Argo quality control manual, version 2.0b. Argo Data Management, 26 November 2004, 23 pp.

Argo Science Team (2000): Report of the Argo Science Team Second Meeting. *Proc. Argo Science Team Second Meeting*, Southampton Oceanography Centre, Southampton, U.K., 35 pp.

Argo Science Team (2001): Argo: The global array of profiling floats. p. 248–258. In *Observing the Oceans in the 21st Century*, ed. by C. J. Koblinsky and N. R. Smith, GODAE Project Office, Bureau of Meteorology, Melbourne.

Bathen, K. H. (1972): On the seasonal changes in the depth of the mixed layer in the North Pacific Ocean. *J. Geophys. Res.*, **77**, 7138–7150.

Bingham, F. M. (1992): Formation and spreading of Subtropical Mode Water in the North Pacific. *J. Geophys. Res.*, **97**, 11,177–11,189.

Cannon, G. A. (1966): Tropical waters in the western Pacific Oceans, August–September 1957. *Deep-Sea Res.*, **13**, 1139–1148.

Cokelet, E. D. and P. J. Stabeno (1997): Mooring observations of the thermal structure, salinity, and currents in the SE Bering Sea basin. *J. Geophys. Res.*, **102**, 22947–22964.

Conkright, M., S. Levitus, T. O'Brien, T. Boyer, J. Antonov and C. Stephens (1998): World Ocean Atlas 1998, CD-ROM

data set documentation. NODC Tech. Rep. 15, Silver Spring, MD, 16 pp.

Conkright, M. E., R. A. Locarnini, H. E. Garcia, T. D. O'Brien, T. P. Boyer, C. Stephens and J. I. Antonov (2002): World Ocean Atlas 2001: Objective analysis, data statistics, and figures, CD-ROM documentation. National Oceanographic Data Center, Silver Spring, MD, 17 pp.

da Silva, A. M., C. C. Young and S. Levitus (1994): *Algorithms and Procedures. Vol. 1, Atlas of Surface Marine Data 1994*. NOAA Atlas NESDIS, 83 pp.

de Boyer Montégut, C., G. Madec, A. S. Fischer, A. Lazar and D. Iudicone (2004): Mixed layer depth over the global ocean: An examination of profile data and a profile-based climatology. *J. Geophys. Res.*, **109**, C12003, doi:10.1029/2004JC002378.

Freeland, H. J. and P. F. Cummins (2005): Argo: A new tool for environmental assessment and monitoring of the world's oceans, an example from the N.E. Pacific. *Prog. Oceanogr.*, **64**, 31–44.

Freeland, H. J., K. L. Denman, C. S. Wong, F. Whitney and R. Jacques (1997): Evidence of change in the winter mixed layer in the Northeast Pacific Ocean. *Deep-Sea Res.*, **44**, 2117–2129.

Hanawa, K. and L. D. Talley (2001): Mode waters. p. 373–386. In *Ocean Circulation and Climate*, ed. by J. Church *et al.*, Academic Press.

Hanawa, K. and Y. Toba (1981): Terms governing temperature and thickness of the oceanic mixed layer and their estimates for sea area south of Japan. *Tohoku Geophys. J.*, **28**, 161–173.

Hautala, S. L. and D. H. Roemmich (1998): Subtropical mode water in the Northeast Pacific basin. *J. Geophys. Res.*, **103**, 13055–13066.

Huang, R. X. and B. Qiu (1994): Three-dimensional structure of the wind-driven circulation in the subtropical North Pacific. *J. Phys. Oceanogr.*, **24**, 1608–1622.

Iwasaka, N., F. Kobashi, Y. Kinoshita and Y. Ohno (2006): Seasonal variations of the upper ocean in the western North Pacific observed by an Argo float. *J. Oceanogr.*, **62**, 481–492.

Kara, A. B., P. A. Rochford and H. E. Hurlburt (2000): Mixed layer depth variability and barrier layer formation over the North Pacific Ocean. *J. Geophys. Res.*, **105**, 16783–16801.

Kara, A. B., P. A. Rochford and H. E. Hurlburt (2003): Mixed layer depth variability over the global ocean. *J. Geophys. Res.*, **108**, 3079, doi:10.1029/2000JC000736.

Kistler, R., E. Kalnay, W. Collins, S. Saha, G. White, J. Woollen, M. Chelliah, W. Ebisuzaki, M. Kanamitsu, V. Kousky, H. van den Dool, R. Jenne and M. Fiorino (2001): The NCEP-NCAR 50-year reanalysis: Monthly means CD-ROM and documentation. *Bull. Amer. Meteor. Soc.*, **82**, 247–268.

Ladd, C. A. and L. Thompson (2000): Formation mechanisms for North Pacific central and eastern subtropical mode waters. *J. Phys. Oceanogr.*, **30**, 868–887.

Levitus, S. (1982): *Climatological Atlas of the World Ocean*. NOAA Prof. Paper 13, 173 pp.

Lukas, R. and E. Lindstrom (1991): The mixed layer of the western equatorial Pacific Ocean. *J. Geophys. Res.*, **96**, 3343–3357.

Marshall, J. C., A. J. G. Nurser and R. G. Williams (1993): Inferring the subduction rate and period over the North Atlantic. *J. Phys. Oceanogr.*, **23**, 1315–1329.

Masumoto, Y., H. Sasaki, T. Kagimoto, N. Komori, A. Ishida, Y. Sasai, T. Miyama, T. Motoi, H. Mitsudera, K. Takahashi, H. Sakuma and T. Yamagata (2004): A fifty-year eddy-resolving simulation of the world ocean: Preliminary outcomes of OFES (OGCM for the Earth Simulator). *J. Earth Simulator*, **1**, 35–56.

Masuzawa, J. (1969): Subtropical Mode Water. *Deep-Sea Res.*, **16**, 463–472.

Miura, T., T. Suga and K. Hanawa (2003): Numerical study of formation of dichothermal water in the Bering Sea. *J. Oceanogr.*, **59**, 369–376.

Monterey, G. and S. Levitus (1997): *Seasonal Variability of Mixed Layer Depth for the World Ocean*. NOAA Atlas NESDIS 14, 100 pp.

Nakamura, H. (1996): A pycnostad on the bottom of the ventilated portion in the central subtropical North Pacific: Its distribution and formation. *J. Oceanogr.*, **52**, 171–188.

Ohno, Y., T. Kobayashi, N. Iwasaka and T. Suga (2004): The mixed layer depth in the North Pacific as detected by the Argo floats. *Geophys. Res. Lett.*, **31**, L11306, doi:10.1029/2004GL019576.

Oka, E. (2005): Long-term sensor drift found in recovered Argo profiling floats. *J. Oceanogr.*, **61**, 775–781.

Oka, E. and K. Ando (2004): Stability of temperature and conductivity sensors of Argo profiling floats. *J. Oceanogr.*, **60**, 253–258.

Oka, E. and T. Suga (2003): Formation region of North Pacific subtropical mode water in the late winter of 2003. *Geophys. Res. Lett.*, **30**, 2205, doi:10.1029/2003GL018581.

Oka, E. and T. Suga (2005): Differential formation and circulation of North Pacific Central Mode Water. *J. Phys. Oceanogr.*, **35**, 1997–2011.

Qiu, B. and R. X. Huang (1995): Ventilation of the North Atlantic and North Pacific: Subduction versus obduction. *J. Phys. Oceanogr.*, **25**, 2374–2390.

Sprintall, J. and D. Roemmich (1999): Characterizing the structure of the surface layer in the Pacific Ocean. *J. Geophys. Res.*, **104**, 23297–23311.

Stommel, H. M. (1979): Determination of water mass properties of water pumped down from Ekman layer to the geostrophic flow below. *Proc. Natl. Acad. Sci. USA.*, **76**, 3051–3055.

Suga, T. and K. Hanawa (1990): The mixed layer climatology in the northwestern part of the North Pacific subtropical gyre and the formation area of Subtropical Mode Water. *J. Mar. Res.*, **48**, 543–566.

Suga, T., Y. Takei and K. Hanawa (1997): Thermostad distribution in the North Pacific subtropical gyre: The central mode water and the subtropical mode water. *J. Phys. Oceanogr.*, **27**, 140–152.

Suga, T., A. Kato and K. Hanawa (2000): North Pacific Tropical Water: Its climatology and temporal changes associated with the climate regime shift in the 1970s. *Prog. Oceanogr.*, **47**, 223–256.

Suga, T., K. Motoki, Y. Aoki and A. M. Macdonald (2004): The

North Pacific climatology of winter mixed layer and mode waters. *J. Phys. Oceanogr.*, **34**, 3–22.

Takeuchi, E. (2006): Studies on the wintertime shoaling of oceanic surface mixed layer. Doctoral dissertation, Graduate School of Science, The University of Tokyo, 109 pp.

Takeuchi, E. and I. Yasuda (2003): Wintertime shoaling of oceanic surface mixed layer. *Geophys. Res. Lett.*, **30**, 2152, doi:10.1029/2003GL018511.

Tully, J. P. (1964): Oceanographic regions and processes in the seasonal zone of the North Pacific Ocean. p. 68–84. In *Studies on Oceanography*, ed. by K. Yoshida, University of Tokyo Press, Tokyo.

Uda, M. (1963): Oceanography of the subarctic Pacific Ocean. *J. Fish. Res. Board Can.*, **20**, 119–179.

Uehara, H., T. Suga, K. Hanawa and N. Shikama (2003): A role of eddies in formation and transport of North Pacific Subtropical Mode Water. *Geophys. Res. Lett.*, **30**, 1705, doi:10.1029/2003GL017542.

Ueno, H., E. Oka, T. Suga and H. Onishi (2005): Seasonal and interannual variability of temperature inversions in the subarctic North Pacific. *Geophys. Res. Lett.*, **32**, L20603, doi:10.1029/2005GL023948.

White, W. B. (1995): Design of a global observing system for gyre-scale upper ocean temperature variability. *Prog. Oceanogr.*, **36**, 169–217.

Wirts, A. E. and G. C. Johnson (2005): Recent interannual upper ocean variability in the deep southeast Bering Sea. *J. Mar. Res.*, **63**, 381–405.

Wong, A. and B. King (2005): Report on first Argo delayed-mode QC workshop. First Argo delayed-mode QC workshop, 8–13 April 2005, Scripps Institute of Oceanography, La Jolla, San Diego, U.S.A., 27 pp.

Wong, A. P. S., G. C. Johnson and W. B. Owens (2003): Delayed-mode calibration of autonomous CTD profiling float salinity data by theta-S climatology. *J. Atoms. Ocean Technol.*, **20**, 308–318.

Yasuda, I., T. Tozuka, M. Noto and S. Kouketsu (2000): Heat balance and regime shifts of the mixed layer in the Kuroshio Extension. *Prog. Oceanogr.*, **47**, 257–278.

Yuan, X. and L. D. Talley (1996): The subarctic frontal zone in the North Pacific: Characteristics of frontal structure from climatological data and synoptic surveys. *J. Geophys. Res.*, **101**, 16491–16508.